


 Cite this: *Chem. Commun.*, 2025, **61**, 17882

 Received 5th July 2025,
 Accepted 13th October 2025

DOI: 10.1039/d5cc03791c

rsc.li/chemcomm

Solvent-induced conformational changes in color-tunable hydrogen-bonded organic frameworks

 Longhao Hu,^a Chaohui Lin,^a Dailin Zeng,^a Xianjiao Qin,^a Xiao-Li Lai,^{ib}
 Lingshan Gong,^{*a} Yingxiang Ye,^{ib}^{*a} Thamraa AlShahrani^{ib}^c and
 Shengqian Ma^{ib}^{*d}

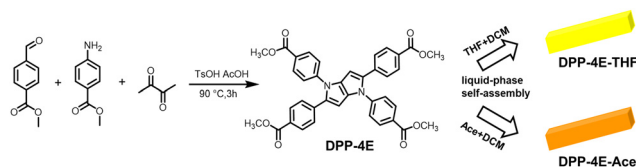
This study reports a pair of conformationally-induced, color-tunable hydrogen-bonded organic frameworks (HOFs) that share identical building blocks but exhibit distinct emission colors—green and orange. A shift of up to 60 nm in their emission wavelengths is observed, which can be attributed to variations in conjugation and energy gap. These results provide in-depth insights into the structural regulation of emission in HOFs.

Hydrogen-bonded organic frameworks (HOFs) are a novel class of crystalline porous materials that self-assemble through hydrogen bonds formed between functional groups, accompanied by weak π - π interactions that stabilize the framework structure of organic molecules.^{1,2} The reversible and weak bonding properties of hydrogen bonds facilitate the construction of dynamic porous HOF materials, enabling the synthesis of a diverse array of HOFs with varying properties by adjusting growth conditions, such as temperature,³ and solvent,^{4,5} from the same organic building unit. In comparison with well-explored crystalline porous materials, such as metal-organic frameworks (MOFs)⁶ and covalent organic frameworks (COFs),⁷ HOFs assembled *via* hydrogen bonding interaction can develop unique functions and applications due to their mild synthesis conditions, designability, and solvent self-assembly.⁸ In addition to being like traditional porous materials used for gas separation,^{9,10} HOFs have been developed for proton conduction,¹¹ temperature sensing,¹² water purification,¹³ and biomedical applications.¹⁴

Luminescent hydrogen-bonded organic frameworks (LHOFs) represent an important branch of multifunctional HOFs, demonstrating significant potential in smart responsive materials.¹⁵ This potential has valuable applications in optical

technologies, including light-emitting devices,¹⁶ fluorescence sensing,^{17,18} and data storage.^{19–21} Tuning the emission wavelength by controlling growth conditions and encapsulating guest molecules to achieve the desired optical properties is a common approach in the fields of laser and fluorescence sensing.^{22,23} For instance, Wang *et al.* used the same fluorescent building block to induce two type of HOFs in different solvents,²⁴ however, the wavelength shifts between the two crystals were found to be insignificant. Subsequently, Lv *et al.* employed a temperature-controlled self-assembly method to prepare a pair of HOFs microcrystals incorporating identical building units. These two HOFs exhibited distinct luminescence colours (blue and green), and they successfully achieved dual-wavelength blue/green laser output.²⁵ Recently, Chi and colleagues enabled programmable luminescence by encapsulating guest molecules of varying lengths through the local dynamics of the ethyl ester chain.²⁶ Although several modulated luminescence strategies have been reported, obtaining two HOFs with significantly different emission wavelengths from the same building block remains a challenge.

In this study, we designed and synthesized tetramethyl 4,4',4'',4'''-(pyrrolo[3,2-*b*]pyrrole-1,2,4,5-tetrayl)tetrabenzoate (DPP-4E; Scheme 1 and Fig. S1)²⁷ as the organic building block for the preparation of color-tunable HOFs. DPP-4E is a luminescent molecule composed of four identical methyl benzoate-modified DPP derivatives (Fig. S5). The ester groups serve as hydrogen bonding sites, connecting adjacent DPP-4E molecules through intermolecular hydrogen bonding to form the final porous framework. The twisting angle between the



Scheme 1 Schematic diagram of the synthesis of DPP-based HOFs Polymorphs.

^a Fujian Key Laboratory of Polymer Materials, College of Chemistry and Materials Science, Fujian Normal University, Fuzhou 350117, People's Republic of China.

E-mail: gonglingshan@fjnu.edu.cn, yingxiangye@fjnu.edu.cn

^b Department of Chemistry, University of North Texas, Denton, Texas 76201, USA.

E-mail: shengqian.ma@unt.edu

^c Department of Physics, College of Science, Princess Nourah bint Abdulrahman University, Riyadh 11564, Saudi Arabia

phenyl arm plane and the pyrrolopyrrole nucleus serves as an indicator of conformational changes, which can influence stacking modes and produce polymorphs, thereby adjusting the emission range. Two bright luminescent HOFs, DPP-4E-THF and DPP-4E-Ace, were obtained by the liquid-phase self-assembly of DPP-4E using different solvents. The crystal structures of these two HOFs exhibit significant differences in the twist angle between the phenyl arm plane and the pyrrolopyrrole core plane, leading to markedly diverse luminescent behaviors. Furthermore, it is worth noting that DPP-4E-THF possesses not only flexible and permanent porous properties but also potential for C_3H_6/C_2H_4 separation.

A pair of hydrogen-bonded isomers was synthesized using a solvent-controlled liquid-phase self-assembly method, utilizing a solvent mixture of DCM and THF to yield yellow crystals of DPP-4E-THF, and a mixture of DCM and Ace to yield orange crystals of DPP-4E-Ace. Both crystallize in the triclinic $P\bar{1}$ space group, with the asymmetric structural unit containing half of the crystallographically independent DPP-4E molecules (Fig. S6). In DPP-4E-THF, the DPP-4E molecule adopts a distorted molecular conformation, with the phenyl group and pyrrolopyrrole unit forming two types of dihedral angles, defined as α and β , measuring 58.8° and 32.3° , respectively (Fig. 1a). Each adjacent DPP-4E molecules form a supramolecular sheet through C-H...O hydrogen bonds (2.71 \AA) between the pyrrolopyrrole nucleus and ester chains and C-H...O hydrogen bonds (2.75 \AA) between ester chains (Fig. 1b). The assembly of these lamellae is further facilitated by a pair of C-H... π interactions (3.08 \AA) (Fig. S8), resulting in the formation of porous structures characterized by one-dimensional (1D) prismatic channels with a pore size of $5.1 \times 6.3 \text{ \AA}^2$ (Fig. 1c). After excluding the guest solvent molecules, the void ratio of DPP-4E-THF was calculated to be 18.2% using PLATON software.²⁸ In comparison, the DPP-4E-Ace lattice is free of solvent molecules, allowing the DPP-4E molecules to achieve a compact packing arrangement. The DPP-4E molecules in DPP-4E-Ace also exhibits a distorted conformation, characterized by

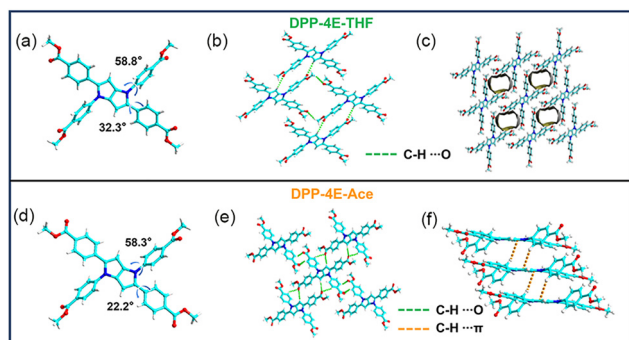


Fig. 1 (a) and (d) Structural unit of DPP-4E in DPP-4E-THF and DPP-4E-Ace. (b) and (e) Structure of the single layer in DPP-4E-THF and DPP-4E-Ace. Solvents are omitted for clarity. Color code: red, O; cyan, C; blue, N; white, H. (c) Packing diagram of DPP-4E-THF along the *a*-axis, with the solvent accessible void space visualized by yellow curved planes generated with a probe of 1.2 \AA . (f) C-H... π interactions between layers in DPP-4E-THF. Distances are given in \AA .

two dihedral angles α and β of 58.3° and 22.2° , respectively (Fig. 1d). Each DPP-4E molecule forms two type of twelve C-H...O hydrogen bonds (2.65 and 2.72 \AA) with four neighboring molecules, resulting in the formation of a supramolecular layer (Fig. 1e). These layers are further assembled into a dense supramolecular network through C-H... π interactions (3.21 \AA) (Fig. 1f).

The experimental powder X-ray diffraction (PXRD) patterns of the as-synthesized DPP-4E-THF and DPP-4E-Ace are in good agreement with the simulated ones (Fig. 2a and b), which illustrates the successful preparation of both samples. As shown in Fig. S9, DPP-4E-THF exhibits a 10.8% weight loss from room temperature to 130°C , mainly due to the loss of THF solvent molecules in the pores, which is in good agreement with the theoretical value of 10.1%; mainly due to the loss of THF solvent molecules in the pores, when the temperature rises to 340°C , a rapid weight loss is displayed, indicating that the structure is beginning to collapse. In contrast, the densely packed DPP-4E-Ace experienced only one weightlessness, and when temperatures exceeded 340°C , the structure began to collapse.

Considering that DPP-4E contains a fluorescent pyrrolopyrrole nucleus, subsequent studies are concentrated on the optical properties of both crystals. When excited at 350 nm , both crystals exhibit significant fluorescence emission, showing strong green (498 nm) and bright yellow (558 nm) emission from DPP-4E-THF and DPP-4E-Ace, respectively. Although composed of the same structural unit, DPP-4E-Ace exhibits a fluorescence redshift of 60 nm compared to DPP-4E-THF (Fig. 2c), which is equivalent to a spectral shift of 2160 cm^{-1} when converted to wavenumbers. To investigate the nature of the different luminescent colors exhibited by these two samples, further analysis was conducted on the molecular conformations of DPP-4E in DPP-4E-THF and DPP-4E-Ace. Comparison of the individual dihedral angles in the

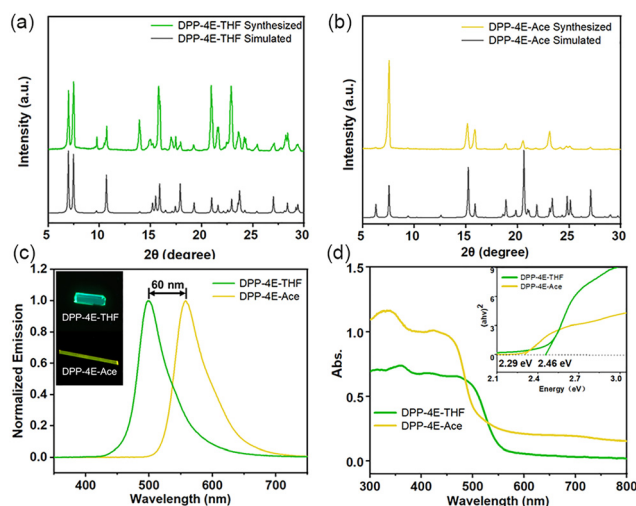


Fig. 2 (a) and (b) PXRD patterns of DPP-4E-THF and DPP-4E-Ace. (c) Normalized PL spectra of DPP-4E-THF and DPP-4E-Ace. Inset: PL optical microscopy images of DPP-4E-THF and DPP-4E-Ace. (d) UV-vis absorption of DPP-4E-THF and DPP-4E-Ace. Inset: the corresponding direct optical band gaps.

two crystal structures revealed that the α in both crystal structures is basically the same (58.8° vs. 58.3°), while the β in DPP-4E-Ace (22.3°) is smaller than that in DPP-4E-THF (32.3°) (Fig. S10). The smaller dihedral angle leads to a more efficient overlap of electrons among all sp^2 hybridized carbon atoms, which produces a higher degree of DPP-4E conjugation in DPP-4E-Ace and ultimately leads to a narrower energy gap between the HOMO and LUMO (Fig. S11),²⁹ which corresponds to the redshift of the emission spectra. Simultaneously, we conducted UV-vis absorption spectroscopy on the solid-state crystalline powder samples. The band gaps of DPP-4E-THF and DPP-4E-Ace were subsequently determined to be 2.29 eV and 2.46 eV, respectively, according to the Kubelka–Munk functional plots.³⁰ The results demonstrate that DPP-4E-Ace exhibits a relatively narrow band-gap (Fig. 2d), which is consistent with the trend observed in the calculated energy gap values.

Furthermore, given the presence of one-dimensional channels in DPP-4E-THF, it has potential application in gas adsorption and separation. The porosity of DPP-4E-THF was initially examined by adsorbing N_2 (77 K) and CO_2 (195 K). For N_2 , no significant adsorption was observed (Fig. 3a). In contrast, the CO_2 adsorption isotherm was negligible at low pressure (6 kPa); however, at pressures between 6 and 15 kPa, the uptake capacity sharply increased to $38\text{ cm}^3\text{ g}^{-1}$. At pressures greater than 15 kPa, the uptake capacity slowly increased to $56\text{ cm}^3\text{ g}^{-1}$. It indicating that the porous framework of DPP-4E-THF has dynamic features. According to the CO_2 adsorption isotherm, the experimental pore volume of DPP-4E-THF was calculated to be $0.11\text{ cm}^3\text{ g}^{-1}$, which is slightly lower than the theoretical value ($0.15\text{ cm}^3\text{ g}^{-1}$) estimated based on the single crystal structure.

Methanol-to-olefin (MTO) is an important method for the industrial preparation of ethylene (C_2H_4).³¹ A key aspect of this process is the separation of propylene/ethylene (C_3H_6/C_2H_4).

The development of efficient and cost-effective technology for C_3H_6/C_2H_4 separation will significantly reduce the energy consumption of the MTO process. Therefore, single-component C_2H_4 and C_3H_6 adsorption isotherms of DPP-4E-THF were collected at 273 K and 298 K (Fig. 3b and c). The single-component adsorption isotherms revealed that the adsorption of C_3H_6 by DPP-4E-THF at both temperatures exhibited a gate-open phenomenon, which commenced at a pressure of 20 kPa. The maximum adsorption capacities were determined to be $25\text{ cm}^3\text{ g}^{-1}$ and $23\text{ cm}^3\text{ g}^{-1}$, respectively. Surprisingly, DPP-4E-THF absorbed a negligible amount of C_2H_4 under the same conditions, which was less than that of any other material that significantly absorbed C_3H_6 . More importantly, the uptake ratios of equimolar C_3H_6/C_2H_4 of DPP-4E-THF reaching up to 33 at 273 K, which is the highest value among the reported porous materials (Fig. 3d).^{32–38} Therefore, DPP-4E-THF is expected to be valuable for industrial applications in the separation of C_3H_6/C_2H_4 mixtures.

In conclusion, this study investigates the color-tunable properties of HOFs, which arise from conformational changes and varying stacking modes. The results demonstrate that the different conformations of DPP-4E in the two crystal structures influence the degree of conjugation, leading to a redshift of up to 60 nm in the emission wavelength. Additionally, the separation performance of DPP-4E-THF for C_3H_6/C_2H_4 was also examined. Notably, the uptake ratios of DPP-4E-THF for C_3H_6/C_2H_4 exceed those of most reported porous materials, highlighting its potential for effective separation. This work also provides a valuable case study for the separation of C_3H_6 and C_2H_4 .

The authors are grateful for financial support from the National Natural Science Foundation of China (grant no. 22301039, 22405043 and 22401048), the Fujian Provincial Department of Science and Technology (grant no. 2024J01451 and 2024J08047) for this work. Partial support from the Robert A. Welch Foundation (B-0027) (S. M.) and Princess Nourah bint Abdulrahman University Researchers Supporting Project (PNURSP2025R1), Riyadh, Saudi Arabia (T. A.) is also acknowledged.

Conflicts of interest

There are no conflicts to declare.

Data availability

The data supporting this article have been included as part of the supplementary information (SI). Supplementary information: Experimental procedures and additional figures and tables. See DOI: <https://doi.org/10.1039/d5cc03791c>.

CCDC 2463084 and 2463085 contain the supplementary crystallographic data for this paper.^{39a,b}

Notes and references

- Z. Zhang, Y. Ye, S. Xiang and B. Chen, *Acc. Chem. Res.*, 2022, **55**, 3752–3766.
- R.-B. Lin, Y. He, P. Li, H. Wang, W. Zhou and B. Chen, *Chem. Soc. Rev.*, 2019, **48**, 1362–1389.

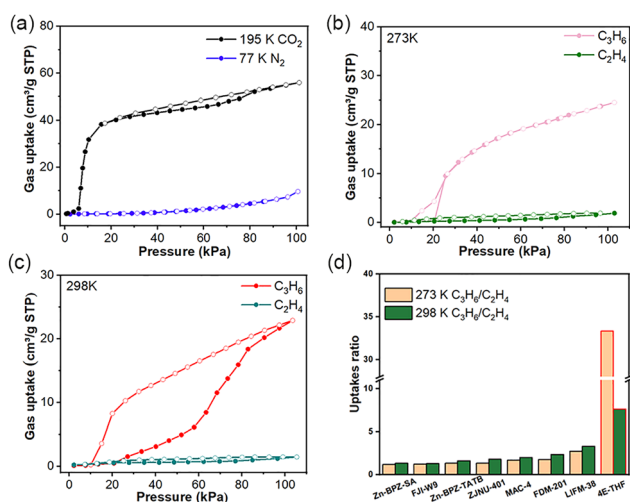


Fig. 3 (a) 77 K N_2 and 195 K CO_2 adsorption isotherms of DPP-4E-THF. (b) and (c) adsorption isotherms of DPP-4E-THF for C_2H_4 and C_3H_6 at 273 and 298 K. Filled and open symbols represent adsorption and desorption, respectively. (d) Comparison of the uptakes ratio of C_3H_6/C_2H_4 among representative porous materials.

- 3 X. Zhang, C. Liu, L. Jiang, Y. Wang, W. Liu and Z. Li, *Cryst. Growth Des.*, 2023, **23**, 1840–1847.
- 4 P. Wei, Z. Zheng, J. Gong, J. Zhang, H. H. Y. Sung, I. D. Williams, J. W. Y. Lam and B. Z. Tang, *Angew. Chem., Int. Ed.*, 2020, **60**, 7148–7154.
- 5 Y. Shi, S. Wang, W. Tao, J. Guo, S. Xie, Y. Ding, G. Xu, C. Chen, X. Sun, Z. Zhang, Z. He, P. Wei and B. Z. Tang, *Nat. Commun.*, 2022, **13**, 1882.
- 6 L. Gong, S. C. Pal, Y. Ye and S. Ma, *Acc. Mater. Res.*, 2025, **6**, 499–511.
- 7 S.-Y. Ding and W. Wang, *Chem. Soc. Rev.*, 2013, **42**, 548–568.
- 8 B. Wang, R.-B. Lin, Z. Zhang, S. Xiang and B. Chen, *J. Am. Chem. Soc.*, 2020, **142**, 14399–14416.
- 9 Y. Cai, J. Gao, J. H. Li, P. Liu, Y. Zheng, W. Zhou, H. Wu, L. Li, R. B. Lin and B. Chen, *Angew. Chem., Int. Ed.*, 2023, **62**, e202308579.
- 10 L. Gong, Y. Ye, Y. Liu, Y. Li, Z. Bao, S. Xiang, Z. Zhang and B. Chen, *ACS Appl. Mater. Interfaces*, 2022, **14**, 19623–19628.
- 11 Y. L. Li, J. F. Lu, Q. Yin, L. Cai, H. J. Jiang, C. Liu, G. Xu and T. F. Liu, *Angew. Chem., Int. Ed.*, 2025, **64**, e202504396.
- 12 X. Liu, Y. Ye, X. He, Q. Niu, B. Chen and Z. Li, *Angew. Chem., Int. Ed.*, 2024, **63**, 202400195.
- 13 L. Hou, C. Shan, Y. Song, S. Chen, L. Wojtas, S. Ma, Q. Sun and L. Zhang, *Angew. Chem., Int. Ed.*, 2021, **60**, 14664–14670.
- 14 S. C. Wang, Q. S. Zhang, Z. Wang, S. Q. Guan, X. D. Zhang, X. H. Xiong and M. Pan, *Angew. Chem., Int. Ed.*, 2023, **62**, e202315382.
- 15 Z. Xiong, S. Xiang, Y. Lv, B. Chen and Z. Zhang, *Adv. Funct. Mater.*, 2024, **34**, 2403635.
- 16 X. Xu, J. Wang and B. Yan, *Adv. Funct. Mater.*, 2021, **31**, 2103321.
- 17 B. Wang, R. He, L.-H. Xie, Z.-J. Lin, X. Zhang, J. Wang, H. Huang, Z. Zhang, K. S. Schanze, J. Zhang, S. Xiang and B. Chen, *J. Am. Chem. Soc.*, 2020, **142**, 12478–12485.
- 18 H. Chen, H. Huang, H. Xu, T. Wu, Y. Xu, X. Ma, W. Yi, G. Chen, S. Huang and G. Ouyang, *Small*, 2023, **20**, 2308716.
- 19 H. Bi, Y. Shi, T. Wang, S. Deng, B. Z. Tang and P. Wei, *Angew. Chem., Int. Ed.*, 2024, **63**, e202409211.
- 20 Y. Lv, J. Liang, Z. Xiong, X. Yang, Y. Li, H. Zhang, S. Xiang, B. Chen and Z. Zhang, *Adv. Mater.*, 2023, **36**, 2309130.
- 21 Q. Huang, K. I. Otake and S. Kitagawa, *Angew. Chem., Int. Ed.*, 2023, **62**, e202310225.
- 22 Y. Lv, J. Liang, Z. Xiong, H. Zhang, D. Li, X. Yang, S. Xiang and Z. Zhang, *Chem. – Eur. J.*, 2023, **29**, e202204045.
- 23 G. Xia, Z. Jiang, S. Shen, K. Liang, Q. Shao, Z. Cong and H. Wang, *Adv. Opt. Mater.*, 2019, **7**, 1801549.
- 24 H. Wang, Z. Bao, H. Wu, R.-B. Lin, W. Zhou, T.-L. Hu, B. Li, J. C.-G. Zhao and B. Chen, *Chem. Commun.*, 2017, **53**, 11150–11153.
- 25 Y. Lv, D. Li, A. Ren, Z. Xiong, Y. Yao, K. Cai, S. Xiang, Z. Zhang and Y. S. Zhao, *ACS Appl. Mater. Interfaces*, 2021, **13**, 28662–28667.
- 26 Q. Huang, X. Chen, W. Li, Z. Yang, Y. Zhang, J. Zhao and Z. Chi, *Chem*, 2023, **9**, 1241–1254.
- 27 Z. Peng, Y. Ji, Z. Huang, B. Tong, J. Shi and Y. Dong, *Mater. Chem. Front.*, 2018, **2**, 1175–1183.
- 28 A. L. Spek, *J. Appl. Crystallogr.*, 2003, **36**, 7–13.
- 29 Z. Hu, G. Huang, W. P. Lustig, F. Wang, H. Wang, S. J. Teat, D. Banerjee, D. Zhang and J. Li, *Chem. Commun.*, 2015, **51**, 3045–3048.
- 30 M. H. Li, Z. Yang, H. Hui, B. Yang, Y. Wang and Y. W. Yang, *Angew. Chem., Int. Ed.*, 2023, **62**, e202313358.
- 31 Y. Zhou, C. Chen, Z. Ji, R. Krishna, Z. Di, D. Yuan and M. Wu, *ACS Mater. Lett.*, 2024, **6**, 1388–1395.
- 32 G.-D. Wang, R. Krishna, Y.-Z. Li, Y.-Y. Ma, L. Hou, Y.-Y. Wang and Z. Zhu, *ACS Mater. Lett.*, 2023, **5**, 1091–1099.
- 33 Y. Rao, X. Li, H. Xi, Z. Jiang, W. Li, H. Zhou, Y. Zhang, C. Wu, Y.-B. Zhang and Q. Li, *J. Mater. Chem. A*, 2025, **13**, 11382–11388.
- 34 G. D. Wang, Y. Z. Li, W. J. Shi, L. Hou, Y. Y. Wang and Z. Zhu, *Angew. Chem., Int. Ed.*, 2023, **62**, e202311654.
- 35 H. Li, Y. Zhou, C. Chen, Y. Li, Z. Liu, M. Wu and M. Hong, *Inorg. Chem.*, 2024, **63**, 21548–21554.
- 36 G. D. Wang, Y. Z. Li, R. Krishna, W. Y. Zhang, L. Hou, Y. Y. Wang and Z. Zhu, *Angew. Chem., Int. Ed.*, 2024, **63**, e202319978.
- 37 J. Li, Z. Song, X. Zhou, X. Wang, M. Feng, D. Wang and B. Chen, *Chem. Sci.*, 2025, **16**, 7411–7417.
- 38 C.-X. Chen, Z.-W. Wei, Q.-F. Qiu, Y.-Z. Fan, C.-C. Cao, H.-P. Wang, J.-J. Jiang, D. Fenske and C.-Y. Su, *Cryst. Growth Des.*, 2017, **17**, 1476–1479.
- 39 (a) CCDC 2463084: Experimental Crystal Structure Determination, 2025, DOI: [10.5517/ccdc.csd.cc2np1br](https://doi.org/10.5517/ccdc.csd.cc2np1br); (b) CCDC 2463085: Experimental Crystal Structure Determination, 2025, DOI: [10.5517/ccdc.csd.cc2np1cs](https://doi.org/10.5517/ccdc.csd.cc2np1cs).